

Degenerate astigmatic cavitiesJ r mie Courtois,¹ Ajmal Mohamed,¹ and Daniele Romanini²¹ONERA–The French Aerospace Lab, 91123 Palaiseau Cedex, France²UJF–Grenoble 1/CNRS, Laboratory of Interdisciplinary Physics, UMR 5588, Grenoble, F-38041, France

(Received 27 June 2013; published 29 October 2013)

At the output of a high-finesse cavity a succession of Lissajous patterns may be observed as the cavity length is finely tuned inside a “degenerate region” around a reentrant spherical configuration. This behavior is ascribed to a small parasitic astigmatism of the cavity mirrors. Simple geometrical optics modeling confirms this hypothesis, and then a more realistic analysis using transverse Gaussian modes reveals that the Lissajous patterns correspond to an organization of the astigmatism-split modes into a finer substructure of degenerate modes relative to that of a reentrant spherical cavity. This provides a thorough understanding of the field patterns observed in the degenerate region, including an intriguing spatial symmetry of the patterns corresponding to opposite displacements with respect to a specific central cavity length. This investigation represents a generalization of the theory of reentrant spherical cavities to the astigmatic case.

DOI: [10.1103/PhysRevA.88.043844](https://doi.org/10.1103/PhysRevA.88.043844)

PACS number(s): 42.15.–i, 42.25.–p, 42.60.–v

I. INTRODUCTION

After more than 30 years of developments, cavity enhanced absorption spectroscopy is still a subject of active research, and the domain of application is steadily expanding. This can be partly attributed to technological progress making available optics of ever higher quality (in particular highly reflective mirrors), and also resulting in new and highly versatile laser systems. New cavity enhanced developments are today possible only through a deeper understanding and a finer exploitation of the properties of high-finesse optical cavities. In particular this concerns transverse modes whose spectral distribution can be controlled by acting on the cavity geometry, and whose population by injected photons can be controlled by acting on the shape and alignment of the excitation laser beam.

Besides cavity enhanced spectroscopy, the question of how the transverse modes of an optical cavity are excited by an incoming Gaussian beam is of more general interest. In particular, determining the coupling coefficients of a laser mode with the cavity modes is a classic problem of optics. As early as 1966, Kogelnik [1] elaborated a model giving an expression for the amplitudes for the first transverse excited Hermite-Gaussian (HG) modes in the case of a perfectly mode matched incoming beam affected by a slight tilt angle with respect to the cavity optical axis. In 1984, Bayer-Helms [2] gave complete expressions for the coupling of transverse cavity modes taking into account both mismatching and misalignments. However, these results are mathematically complex and do not appear to be computationally efficient. More recently, in 1996, Lehmann and Romanini [3] proposed, in their first Appendix, a recursion relationship permitting to involve a generic (elliptic and astigmatic) misaligned Gaussian beam together with arbitrary incident waist size and arbitrary waist position. These developments have been thereafter revisited by Romanini [4] who corrected for some errors, making the results exploitable, and generalized the recursive analytical relations to astigmatic and elliptic cavities and beams. This allows the fast and accurate modeling of real systems with up to thousands of excited transverse modes. In particular, the self-consistency and numerical stability of the model has been highlighted by simulating the electric field

pattern produced in the cavity for an incoming off-axis beam at a frequency resonating with one of the N degenerate groups of modes of a spherical reentrant cavity [4]. In this case, studied initially by Herriott *et al.* in 1964 using geometrical optics arguments [5], the beam spatially overlaps with itself after N cavity round trips, where N is the so-called reentrant order of the chosen resonator configuration. As a result, one obtains a simulated transverse cavity output pattern with N spots, reproducing with wave optics [4] the result from ray tracing.

In this paper, we apply these recent modeling developments exploiting the superposition of excited transverse cavity modes, as well as ray tracing, to realistic cavities affected by mirror astigmatism, which appears to be hardly avoidable under normal experimental conditions. This allows a full understanding of the physics leading to the existence of a succession of Lissajous patterns appearing at the resonator output as its length is finely detuned in the vicinity of a spherical reentrant configuration. Interestingly, in such *degenerate regions* of the cavity length, it is found that the successive transverse field patterns can exhibit a symmetric behavior with respect to a central mirror separation: Modeling performed herein will provide a complete understanding of this observation.

It is remarkable, according to our bibliographic search, that only geometrical optics arguments were applied to analyze the cavity output field profiles, starting back in 1965 with the pioneering paper of Herriott and Schulte [6]. Even though later extended to twisted astigmatic multipass cells [7], allowing to investigate a wide variety of circulation patterns (with the aim of reducing multipass cell volumes as well), no identification of the existence of degenerate regions for transverse Lissajous profiles can be found in the literature. Regarding laser resonators, only Chen *et al.*, to the best of our knowledge, have been employing the quantum theory to reconstruct high-order transverse patterns observed in a microchip laser [8,9] having accidental astigmatism. They performed accurate systematic numerical calculations based on the similarity between the spherical resonator and the quantum stationary coherent states of the commensurate anisotropic two-dimensional harmonic oscillator; however, the

analogy appears too complex and unsuited for providing a clear understanding of the physical phenomena investigated here. In contrast, we propose an in-depth analysis based on the superposition principle [3] as a description together significantly simpler and physically intuitive, which fully accounts for the formation of a succession of Lissajous patterns around the reentrant configuration of the unperturbed spherical cavity. These patterns will be shown to correspond to the organization of the cavity transverse modes in degenerate groups clustered around the single degenerate group that would occur in the limit of a reentrant spherical cavity. This present investigation therefore generalizes and extends the theory of reentrant cavities to the astigmatic case. Apart from weak transverse mode coupling in degenerate cavities caused by mirror surface aberrations [10–12], our experience is that a small parasitic astigmatism is the most common and effective situation which causes a splitting of modes (larger than their spectral width for higher finesses) when one tries to approach the reentrant configuration. This fact is confirmed by the close match we find between the observed Lissajous patterns and the results from modeling an astigmatic cavity.

II. EXPERIMENTAL PROCEDURES AND OBSERVATIONS

Our experimental off-axis cavity injection scheme is presented in Fig. 1(a). As in our previous work [13], we use an external cavity diode laser (ECDL; Toptica DL-100) emitting around 765 nm as a narrow-linewidth continuous wave (cw) tunable source. The setup includes a Faraday optical isolator to prevent undesired optical feedbacks toward the ECDL, followed by a fiber coupling system. The divergent beam leaving the fiber is focused by a $f = 11$ mm lens whose distance from the input cavity mirror is close to what is needed to match a

TEM₀₀ spatial beam to the corresponding cavity mode. After this mode matching lens, two steering mirrors [not presented in Fig. 1(a)] allow to adjust for an off-axis cavity injection.

Our cavity is formed by two concave mirrors (Layertec GmbH with a specified reflectivity of 99.97% (finesse $\sim 12\,000$) at 765 nm, a 1-m radius of curvature, and a 12.7-mm diameter. All results presented here are obtained with a cavity length of ~ 293 mm finely adjustable over a ± 2 -mm range. This corresponds to a $K/N = 1/4$ fractionally degenerate spherical resonator, i.e., a Herriott spherical configuration with a fourfold reentrant trajectory, and four output beams generated off each mirror.

Light patterns transmitted by the cavity are directly imaged onto a charge-coupled device (CCD) camera. The laser frequency is rapidly swept over almost 15 GHz with a 200-Hz triangular current modulation (4.2 THz/s), providing frequency-averaged cavity output patterns.

The observed transmission pattern exhibits Lissajous profiles at cavity output when the cavity length L is finely tuned around a specific cavity length, as displayed in Fig. 1(b). As we will see, this indicates that the cavity is not perfectly spherical, and that a weak residual astigmatism frustrates the observation of $N = 4$ distinct spots on both mirrors for a single reentrant length value. Each successive sharp pattern is observed by incrementing the cavity length by $\Delta L \sim 0.2$ mm. Between two subsequent sharp patterns, the output appears irregular, dim, and vague. Our observations lead to isolating a pattern that occurs for a specific L_{sym}^- (the “symmetric” cavity length) that has a “X” profile on M_2 . An intriguing spatial symmetry of the Lissajous patterns is, besides, clearly observed for cavity lengths detuned around this specific cavity length: The same pattern is obtained at $+M\Delta L$ and $-M\Delta L$ except for a 90° rotation and a reflection. It is worth pointing out that the

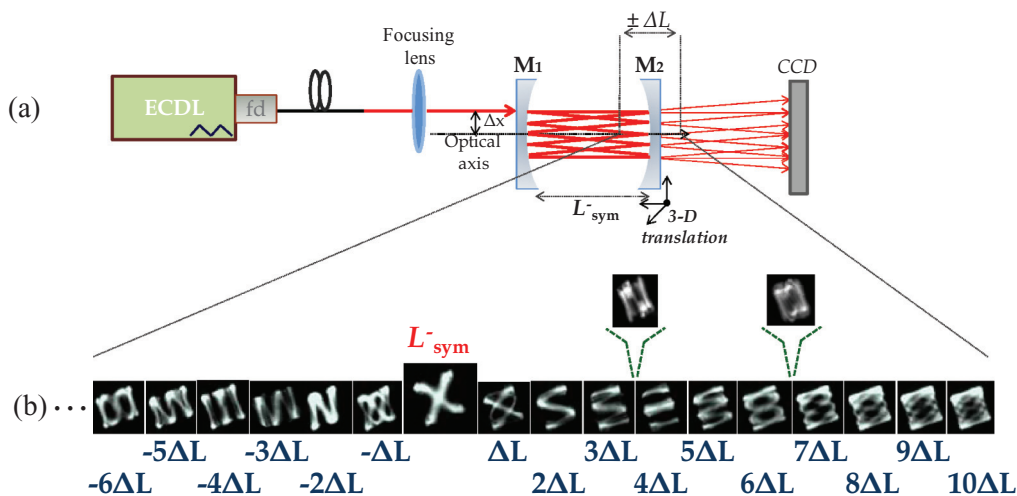


FIG. 1. (Color online) (a) Off-axis cavity injection setup. ECDL: external cavity diode laser. Fd: Fibredock. $M_{1,2}$: high-reflectivity cavity mirrors. CCD: imaging camera. (b) Transverse patterns observed at the cavity output when the cavity length is finely adjusted in the vicinity of the “symmetric” length L_{sym}^- , which only depends on astigmatism [see Eq. (5)]. In the present experiment, this cavity length roughly corresponds to that of a $(N, K) = (4, 1)$ reentrant configuration of a spherical cavity. The cavity length detuning ΔL between two successive sharp Lissajous patterns is found to be approximately 0.2 mm, which from modeling should correspond to an astigmatism of $\Delta R/R \sim 0.4\%$, as confirmed by previous ring-down measurements on this same cavity [13]. Also are highlighted, on the right-hand side, two examples of irregular and vague patterns observed between two successive sharp patterns.

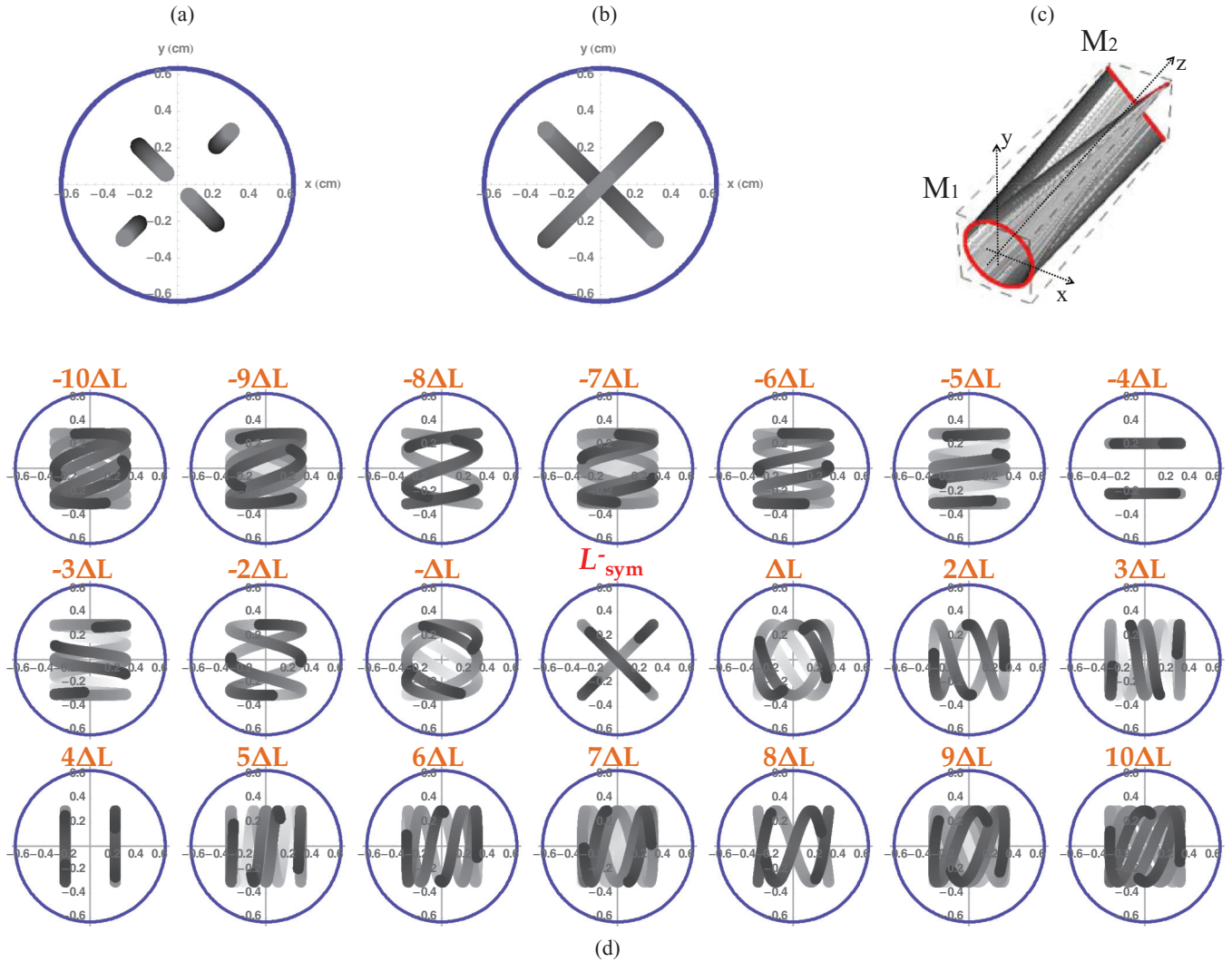


FIG. 2. (Color online) Examples of simulations obtained with ray tracing by the $ABCD$ -matrix formalism. In (a) and (b) are compared beam spots patterns simulated on the output mirror for different cavity finesses, respectively 2090 and 12 080, when identical cavity length [the symmetric cavity length L_{sym}^- expressed by Eq. (5)] and identical cavity injection parameters $(x_0, y_0, x'_0, y'_0) = (-0.3 \text{ mm}, 0 \text{ mm}, 0.17^\circ, -0.41^\circ)$ are used. In (c) is modeled a three-dimensional ray trajectory, in the same case as (b), highlighting the patterns obtained on the two cavity mirrors at the interesting L_{sym}^- cavity length. In (d) are patterns computed when the cavity length is incremented (respectively decremented) stepwise by $\Delta L = \pm 0.147 \text{ mm}$ with respect to the X pattern at $L_{\text{sym}}^- = 292.89 \text{ mm}$ according to Eq. (5) for $R_x = 1002 \text{ mm}$ and $R_y = 998 \text{ mm}$. Cavity injection conditions are kept constant.

exact shape of these patterns depends on the incident beam alignment, once a cavity length that gives a sharp pattern has been fixed. For example, the X pattern can also be continuously changed into an “O” profile (passing through crossed ellipses). Actually these two patterns are complementary as they are produced at opposite cavity sides, consistent with ray tracing represented in Fig. 2(c), and with modal simulations based on Ref. [4] and further developed below. For our setup, i.e., for a given cavity injection and cavity astigmatism as well, these sharp patterns are only observed in a $\pm \sim 2\text{-mm}$ cavity length range that we will refer to as a *degenerate region*. As we will see, other cavity length intervals, where a similar succession of Lissajous patterns should be observed (except both for the special X-O profiles occurring at L_{sym}^- and the intriguing spatial symmetry around it), do exist and are always centered on configurations that are reentrant in the limit of a spherical cavity.

III. ASTIGMATIC CAVITY, LISSAJOUS PROFILES, AND DEGENERATE REGIONS

A. Degenerate cavities and astigmatism: Generalities

Let us recall briefly the framework for degenerate cavities. Assuming small angles between the propagation axis of the incoming beam and the optical cavity axis z for which the paraxial approximation is satisfied, the spatial HG modes native from a spherical resonator are expressed as [14]

$$\begin{aligned}
 E_{mn}(x, y, z) &= E_0 \frac{\omega_0}{\omega(z) \sqrt{2^{m+n-1} \pi m! n!}} H_m \left[\frac{\sqrt{2}x}{\omega(z)} \right] H_n \left[\frac{\sqrt{2}y}{\omega(z)} \right] \\
 &\times \exp \left[-\frac{x^2 + y^2}{\omega(z)^2} \right] \exp \left\{ -ik \left[\frac{(x^2 + y^2)}{2r(z)} + z \right] \right. \\
 &\left. + i(m+n+1)\varphi(z) \right\}. \quad (1)
 \end{aligned}$$

Here $\omega(z) = \omega_0[1 + (z/z_R)^2]^{1/2}$ is the transverse beam radius at the z position; ω_0 and $z_R = \pi\omega_0^2/\lambda$ are, by definition, the beam transverse dimension at the waist and the confocal or Rayleigh length, respectively; $k = 2\pi/\lambda$ is the wave vector in vacuum while $r(z) = z[1 + (z/z_R)^2]$ and $\varphi(z) = \arctan(z/z_R)$ are, respectively, the wave-front curvature radius and the Gouy phase shift. Functions $H_{m,n}(\cdot)$ are the Hermite polynomials. From the cavity round-trip self-consistency condition applied to these spatial modes, the resonator eigenfrequencies $\nu_{q,mn}$ are derived [14]:

$$\nu_{q,mn}^{\text{Spherical}} = \frac{c}{2L} \left[q + (m+n+1) \frac{\theta}{2\pi} \right], \quad (2)$$

where $\theta = 2\arccos(g_1g_2)^{1/2}$ represents the Gouy phase shift accumulated by the TEM₀₀ mode over one cavity round trip and $g_{1,2} = 1 - L/R_{1,2}$ are the geometric cavity parameters, with $R_{1,2}$ the radii of curvature for the two mirrors. For every transverse mode of indices m and n , we see from Eq. (2) that the resulting spectrum consists of combs of longitudinal modes (as a function of q) sharing the same basic spacing given by $\nu_{q+1,mn} - \nu_{q,mn} = \Delta\nu_L = c/2L$, the cavity free spectral range (FSR). On the other hand, the transverse mode spacing (when changing m or n by 1) is $\Delta\nu_T = \Delta\nu_L\theta/2\pi$. For special cavity lengths such that the round-trip TEM₀₀ Gouy phase shift is a low-order rational relative to 2π (that is, $\theta = 2\pi K/N$ where K and N are two small integers with no common factor verifying $0 < K < N$), the resonant frequencies become

$$\nu_{q,mn}^{\text{Spherical}} = \frac{c}{2LN} [Nq + K(m+n+1)]. \quad (3)$$

In this case, the cavity exhibits degeneracy involving different transverse mode families. Indeed, incrementing (decrementing) the longitudinal mode index q by K while simultaneously decrementing (incrementing) the sum of the transverse mode indices ($m+n$) by N leaves the frequency unchanged. Consequently, there exist N degenerate groups of modes being excited between two subsequent TEM₀₀ resonances. This so-called fractionally degenerate resonator, described above by wave optics, corresponds to a reentrant spherical resonator in a description based on geometrical optics [5]. In this latter representation, a paraxial ray follows a trajectory that closes on itself after N cavity round trips (note that K represents the number of transverse cycles, i.e., how many times the ray trajectory cycles around the optical axis), irrespective of the input beam injection positions and slopes. This is a direct result of the fact that, in the $ABCD$ -matrix formalism (ruling Gaussian mode propagation and ray tracing as well), the N th power of the round-trip cavity propagation matrix is unity, which implies that the reentrant resonator preserves input beam coordinates and slopes together after N cavity round trips.

Recently, we published [13] cavity ring-down spectroscopy results exploiting degenerate resonators and off-axis injection in order to take advantage of the cavity transverse mode structure and, in doing so, refine the spectral domain sampling grid. There, we discussed the successful observation of N distinct spots on the cavity mirrors only for a moderate cavity finesse ($F \sim 2000$), while the observation of the above Lissajous figures occurred with the higher-reflectivity mirrors also used in this study ($F \sim 12\,000$). From the selective beating

note measurements of TEM₀₁ and TEM₁₀ modes (appearing on the ring-down events under specific experimental condition), we were capable of estimating the slight astigmatism suggested by the observed Lissajous figures [13], and we found (supposing identical mirrors) a $|R_y - R_x|$ value of about 4 mm relative to the specified curvature value $R = 1000$ mm, i.e., $\Delta R/R = 0.4\%$. To allow direct comparison with the experience we shall then assume, in the following, an optical cavity formed of two identical mirrors with radii of curvature of 1002 and 998 mm along the x and y transverse directions, respectively. One could argue that this is not a realistic situation since the astigmatism of the cavity mirrors is certainly not equal, nor oriented the same way, unless we made some effort for that to be the case. However, let us consider a generic astigmatic cavity made of two mirrors with the same specified curvature but affected by small parasitic variations of the curvature, along different transverse directions. It is easy to show that, after expansion to the first order in these variations, the round-trip matrix of this cavity can be rewritten as the matrix of a cavity with mirrors possessing the same variation of the curvature radius along a common transverse direction (which does not coincide with any of the original directions).

For such an astigmatic cavity, in place of Eq. (2) eigenfrequencies are given as

$$\nu_{q,mn}^{\text{Astigmatic}} = \frac{c}{2L} \left[q + \left(m + \frac{1}{2} \right) \frac{\theta_x}{2\pi} + \left(n + \frac{1}{2} \right) \frac{\theta_y}{2\pi} \right], \quad (4)$$

where it appears that each transverse dimension x, y has its own round-trip Gouy phase shift expressed by $\theta_{x,y} = 2\arccos(1 - L/R_{x,y})$. We will see below that for specific values of L close to a reentrant configuration, this expression allows for the degeneracy of transverse modes in finely spaced subgroups around the frequencies where the reentrant spherical cavity would present a single degenerate group of modes. Further, we will also see that this organization of modes in degenerate subgroups corresponds to the generation of Lissajous patterns, both in geometrical optics and in wave optics.

In analogy with Eqs. (2) and (3), one would be tempted to consider the cavity configurations such that the Gouy phase shifts are a ratio of small integers: $\theta_x = 2\pi K_x/N$, $\theta_y = 2\pi K_y/N$. The result would be that modes with the same value of $Nq + mK_x + nK_y$ are degenerate in frequency, and one would also expect that the intracavity trajectory traces out a Lissajous pattern, as discussed by Herriott *et al.* [6] and later extended by McManus *et al.* [7] when accounting for the twist of the astigmatic mirror axes about the central cavity axis. However, this condition cannot be met close to a configuration corresponding to the reentrant spherical cavity, as we are considering here. Like R_x and R_y , θ_x and θ_y have very similar values, thus their ratio may correspond at best to a ratio of quite large integers (which cannot correspond to the observed low-order Lissajous patterns). From consideration of transverse modes frequencies, we will see that the right condition is to be written as $N\theta_x/2\pi - 1 = K_x$, $N\theta_y/2\pi - 1 = K_y$.

B. Geometrical optics analysis

Herriott *et al.* have shown that, in the presence of cavity astigmatism, an intracavity light beam may propagate back and forth between the two mirrors in a manner such that its impact

spots on the mirrors trace out a Lissajous pattern [6]. This replaces the observation of simple elliptical spot trajectories for a spherical cavity [5]. It comes about by considering that the transverse coordinates of the n th impact spot on the mirror after injection are $(x_n, y_n) = (A \sin(n\theta_x/2 + \alpha), B \sin(n\theta_y/2 + \beta))$, where A , B , α , and β are constants including injection conditions (input beam coordinates and slopes) as well as mirror spacing and focal lengths. As defined earlier, θ_x and θ_y are the Gouy phase shifts and depend on the cavity geometry and on the mirror curvatures in particular.

Lissajous patterns like those in Fig. 1(b) could be observed for high-enough mirror reflectivities [13]. This fact can be understood by considering that the modest mirror astigmatism demands many round trips before becoming manifest as a walk off of the reflected spots from a basic elliptic trajectory to give rise to a Lissajous figure. To illustrate this point we compare in Figs. 2(a) and 2(b) two calculated spot patterns obtained when one varies the mirror reflectivity from 99.85% to 99.97%. The corresponding cavity free photon lifetimes, i.e., respectively, 0.65 and 3.25 μ s, enable the circulating beam to bounce about 667 and 3333 times on each mirror, respectively. For the low-finesse cavity case, as in Fig. 2(a), beam spots are still roughly describing an ellipse, whereas the Lissajous transverse pattern imposed by the mirror astigmatism is fully developed when the cavity finesse is high enough to allow sweeping the spots trajectory until it comes back to the initial position. This closure of the Lissajous pattern occurs only for specific cavity lengths, independently of the input beam parameters.

Figure 2(d) also displays Lissajous patterns simulated when one varies the cavity length in the vicinity of a central specific value L_{sym}^- . The characteristic shape of this pattern observed for this cavity length obviously depends on the cavity injection parameters, and herein both the input beam coordinates and slopes are chosen as needed if we were expecting to observe on the mirrors a circular trajectory of the reflected spots in the hypothetical case of a spherical cavity [5]. However, it can be shown that in order to obtain the X and the O patterns that are characteristics of this cavity configuration, two mirror separations are possible:

$$L_{\text{sym}}^{\pm} = R_x R_y \frac{R_x + R_y \pm \sqrt{2R_x R_y}}{R_x^2 + R_y^2}. \quad (5)$$

They arise from Gouy phases satisfying the specific conditions $\theta_x - \pi/2 = -(\theta_y - \pi/2)$, so that both an ellipse and a cross trajectory of the reflected beam are obtained on the mirrors. Figure 2(c) shows an example of the evolution of this beam trajectory within the cavity. For our mirror curvatures, these specific patterns are found for $L_{\text{sym}}^- = 292.89$ mm and $L_{\text{sym}}^+ = 1707.09$ mm. We note that by using $R_x = R_y$, in Eq. (5), L_{sym}^- becomes equal to the conventional reentrant resonator $L_r = R[1 - \cos(\pi K/N)]$, i.e., 292.89 mm for mirrors with radius of curvature $R = 1000$ mm exactly, as derived for a spherical $(N, K) = (4, 1)$ reentrant cavity.

Other patterns presented in Fig. 2(d) match our laboratory observation of Fig. 1, i.e., a succession of Lissajous profiles at successive cavity lengths separated by a constant step size $\Delta L = 0.147$ mm. In particular, for symmetric cavity length variations $\pm M \Delta L$ around L_{sym}^- , transverse patterns are linked

by a spatial ($-i$) transformation, i.e., a mapping of the beam spots' coordinates expressed as $x_n(L_{\text{sym}} + \Delta L) = y_n(L_{\text{sym}} - \Delta L)$, $y_n(L_{\text{sym}} + \Delta L) = -x_n(L_{\text{sym}} - \Delta L)$.

To resume, the observed sharp patterns can be associated to impact spot trajectories that are closing during the cavity photon lifetime. On the other hand, the irregular and vague patterns result from spots that keep running on the mirror surfaces without tracing a closed trajectory. The fact that so many different Lissajous patterns are generated by varying the cavity length over a small interval is due to the fact that $(N\theta_x/2\pi - 1)/(N\theta_y/2\pi - 1)$ varies rapidly since it is the ratio of two quantities which are close to zero.

C. Wave optics analysis

After the previous straightforward geometrical optics picture, we now aim at considering a more complete description enabled by wave optics. This involves excitation of transverse cavity modes by a Gaussian-profile beam incident on the optical resonator, and we can apply the framework developed in [4] for realistic cavities affected by small parasitic astigmatism. The excited intracavity field is then written as a sum over projection coefficients times the corresponding mode functions and the corresponding frequency comb of resonances (Airy formula in the astigmatic case as a function of the round-trip phase shift $\varphi = 2\pi 2L\lambda = \omega 2L/c$):

$$E_{mn}^A(x, y, z, \varphi) = \sum_m \sum_n C_{mn} E_{mn}^A(x, y, z) \frac{T}{1 - R \exp[i\varphi]}, \quad (6)$$

where R , $T = 1 - R - l$, and l are the familiar intensity mirrors' reflectivity, transmission, and losses, respectively. The projection coefficients C_{mn} of the incoming spatial Gaussian beam profile E_{00}^B onto the transverse cavity modes E_{mn}^A are given by the overlap integral $\iint E_{00}^B(x, y) E_{mn}^{A*} dx dy$ which may be calculated on any plane transverse to the cavity axis z . E_{mn}^{A*} is the complex conjugate of the TEM _{mn} astigmatic cavity eigenmode expressed by Eq. (1) modified to allow for independent waist size, wave-front curvature radius, and Gouy phase for x and y . Analytical expressions for an efficient calculation of the C_{mn} coefficients are provided in Ref. [4].

In Fig. 3(a) is an example of the distribution of the absolute values of the coupling coefficients $|C_{mn}|$ for a Gaussian beam incident off axis on a slightly astigmatic cavity. The figure caption gives details about cavity and incident beam parameters. Note that the values of the coupling coefficients are independent on the transverse plane where they are calculated [4]. In Fig. 3(b) is a numerical application of Eq. (6) to present the cavity excitation field profiles modeled on planes $z = 0$ (input mirror) and $z = L$ (output mirror) for the cavity length $L_{\text{sym}}^- = 292.89$ mm as given by Eq. (5). These clearly match the transverse patterns obtained by geometrical optics (Fig. 2) and by experimental observation [Fig. 1(b)]. We also display, in Figs. 3(c) and 3(d), examples of cavity excitation field profiles obtained for two cavity lengths detuned by $\Delta L = \pm 0.585$ mm away from L_{sym}^- . It thus appears, for identical cavity length variations $\pm M \Delta L$ as well as identical cavity and injection beam parameters, that modeled electric field profiles exhibit the observed behavior already modeled by geometrical optics.

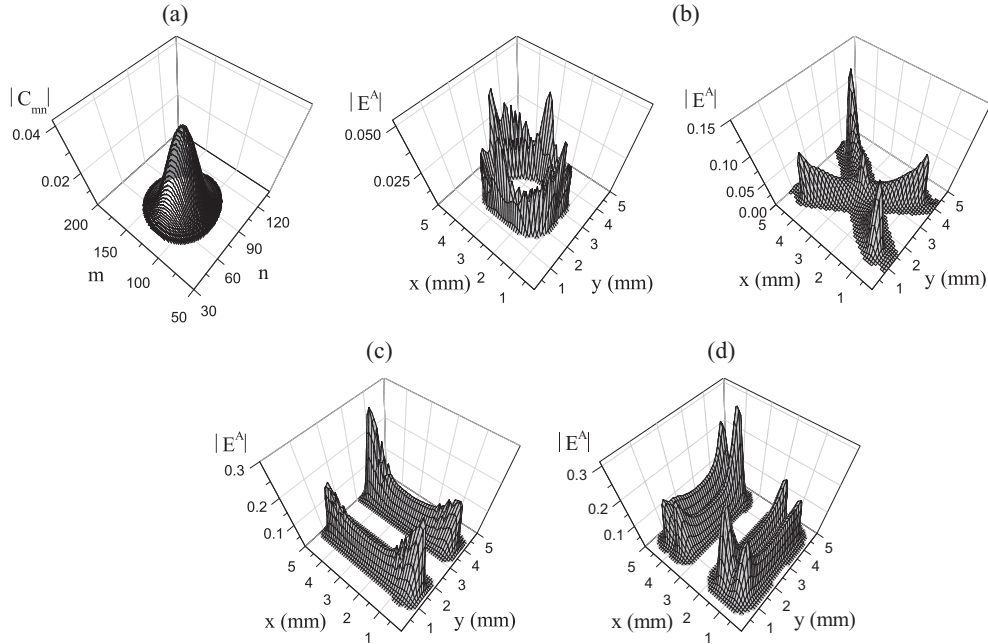


FIG. 3. In (a) is an example of distribution of the absolute values of the projection coefficients $|C_{mn}|$ as a function of the transverse numbers m and n for a cavity length of 292.89 mm made of two identical mirrors with radii of curvature $R_x = 1002$ mm and $R_y = 998$ mm. Here we chose an incident beam that is mode matched to the cavity, then misaligned in position and angle in the same manner as in Fig. 2, i.e., with $(x_0, y_0, x'_0, y'_0) = (-0.3$ mm, 0 mm, $0.17^\circ, -0.41^\circ)$. In (b) are the transverse field distributions simulated at the symmetric cavity length L_{sym} on both the input and output mirrors, respectively. Plots (c) and (d) show two patterns modeled at cavity output ($z = L$) for $L_{\text{sym}} \pm 0.588$ mm, which correspond to $\pm 4\Delta L$ relative to Fig. 2(d).

However, the fact that one can see slight discrepancies between experimental and simulated patterns, e.g., respectively, the “three-bar” patterns at $\pm 4\Delta L$ in Fig. 1(b) against the “two-bar” patterns at $\pm 4\Delta L$ in Fig. 2(d) and Figs. 3(c) and 3(d), is partly due to differences in the input beam parameters. Modeling can show that the three-bar pattern is created on the input mirror rather than on the output mirror as depicted. It is possible that small alignment variations during the experimental recording took place and different figures may have a varying degree of sensitivity to these small variations. Another point that is to be taken into account is that “higher-order” deformation of the mirror surfaces may contribute to distort the observed patterns away from the calculated ones. Still, the good general agreement indicates that astigmatism is by far the dominating mirror defect.

Finally, we remark that all the patterns modeled in Figs. 3(b)–3(d) result practically from the same projection coefficients whose absolute values are represented in Fig. 3(a). Indeed, the variation of the superposition integral giving these coefficients is small for the small cavity length changes considered here. The differences in the observed profiles, however, arise from the interference between the transverse cavity eigenmodes excited by the scanning laser field. Interference can occur and produce structured and stationary field patterns only if at least some of the excited modes are degenerate. Indeed, as we are going to illustrate shortly, even a fine modification of the cavity length may induce Gouy phase shifts which make the excited transverse modes degenerate in groups.

As displayed in Fig. 4(a), the (N, K) reentrant condition corresponds, before introducing the astigmatism, to a frequency

degeneracy of the TEM_{mn} modes into N groups [3], leading to N cavity transmission peaks uniformly distributed over the cavity FSR [see Eq. (3)]. This corresponds to a reentrant beam passing N times around the cavity and cycling K times around the optical axis before overlapping with itself, as we mentioned earlier. It is important to note a surprising fact, i.e., that an incident beam of varying frequency coming in resonance with any of the N groups of degenerate modes will produce a superposition of these modes always corresponding to the same trajectory of N impact spots on the mirrors. Only the field phase distributions will be different when exciting one or another of these N groups of modes [4]. Therefore, even if the incident beam frequency tunes across several cavity FSRs as in our experiment, or else if the beam is polychromatic, the N spots pattern is still readily observable. Therefore, even if the incident beam frequency tunes across several cavity FSRs as in our experiment, or else if the beam is polychromatic, the N spots pattern is still identically produced.

In the presence of astigmatism, the cylindrical symmetry breaks and the degeneracy is lifted according to Eq. (4). Thus, for each of the N resonances, the transmission function of the astigmatic cavity presents a bell-shaped quaresonance as visible in Figs. 4(b) and 4(c) when L is close to L_{sym}^- , i.e., a packet of individual transverse resonances which may present a fine structure made of subgroups of degenerate modes, as in Fig. 4(b). It turns out that the width of this spectral envelope of dispersed modes is proportional to the highest transverse mode order being excited. For an injection close to the optical axis, thus involving low-order transverse modes, the quaresonance envelope width collapses, and in

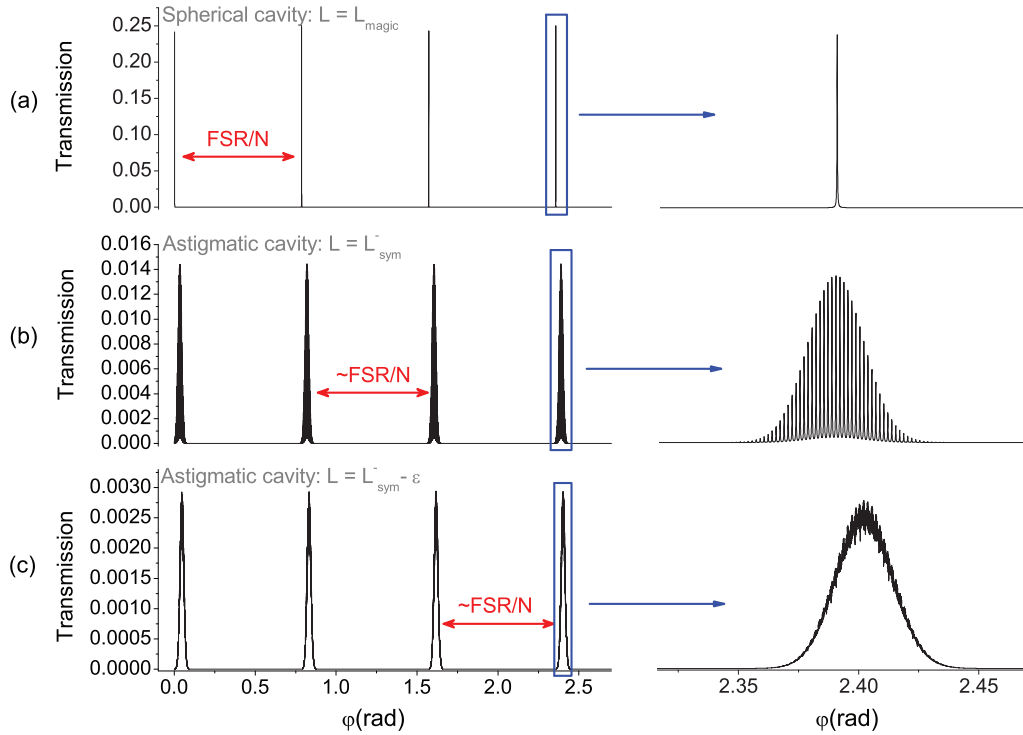


FIG. 4. (Color online) Modeling of the cavity transmission as a function of the phase shift. In (a) the cavity is perfectly spherical with a mirror-to-mirror separation that satisfies the reentrant condition $L_r = R [1 - \cos(\pi K/N)]$ in the case of a $(N, K) = (4, 1)$ reentrant cavity; whereas a small astigmatism ($R_x = 1002$ mm and $R_y = 998$ mm) has been introduced in (b) and (c). All three examples involve identical beam injection parameters and cavity finesse (same as in Figs. 2 and 3). Case (b) corresponds to L_{sym}^- , which is a cavity length that leads to the sharp X-O Lissajous profiles as already plotted in Figs. 2(b), 2(c), and 3(b) using geometrical and wave optics theories, respectively. On the other hand, case (c) corresponds to an irregular and vague profile.

the case of degenerate subgroups only one of these may remain (and will present the same width as a single, isolated, cavity mode). Conversely, the more off axis is the injection the wider becomes the spectral envelope of the quasiresonances.

To better understand this behavior, we should consider the frequency evolution of the transverse modes with L . At first sight one would expect different slopes for modes with the same transverse order $m+n$, since $\partial v(q, m, n)/\partial L = (m + 1/2)\partial\theta_x/\partial L + (n + 1/2)\partial\theta_y/\partial L$. In practice, this difference in slope is negligible (it is 0.26% for the mirror curvatures given above) and the mode splitting by the different values of θ_x and θ_y is the dominant effect [as of Eq. (4)]. Figure 5 presents the normalized (with respect to cavity FSR) frequency separation $[\Delta v(q, m, n)/\Delta v_L]$ of transverse modes with respect to the TEM_{00} mode, plotted as a function of the cavity detuning in the vicinity of L_{sym}^- . The $[]$ indicate that we are taking the fractional difference with respect to the nearest integer (for example, $[1.2] = 0.2$ and $[0.9] = -0.1 \dots$), which avoids having to choose the right value of the longitudinal order q that makes a resonance of a transverse mode comb with given m, n to fall into the chosen FSR interval. $[\Delta v(q, m, n)/\Delta v_L]$ can then be calculated for $q = 0$ and gives the position of the cavity transmission peaks for the transverse modes with considered m, n values, on the vertical axis of Fig. 5, as a function of the cavity length, on the horizontal axis. Each set of parallel lines of the same color and style corresponds to modes with $m+n$ equal to a multiple of N ($= 4$ as before). The vertical axis is zoomed on a small spectral region around 0, where are

visible only modes $m+n = Ni$ with $i = 0, 1, 2, 3, \dots$ which lie close to the TEM_{00} mode. Indeed, modes with $m+n = N(i+1), N(i+2), N(i+3)$, form groups which are located at $1/4, 1/2$, and $3/4$ of the FSR, respectively. For clarity, only the first five transverse families, i.e., with $i = 0, 1, 2, 3, 4$, have been represented. While in the straightforward spherical cavity case the modes sharing an identical $m+n$ transverse order are degenerate and shift together at the same rate with L , here these modes are nondegenerate but still evolve at a very similar rate, as visible in Fig. 5 where lines of the same color and style for modes of the same order are parallel.

The most interesting feature revealed by Fig. 5 is that, as L is finely tuned around L_{sym}^- , there are cavity lengths for which different transverse modes cross simultaneously. In the same way as the reentrant cavity length L_r allows for the degeneracy and the superposition of the transverse modes necessary to produce a N -fold reentrant trajectory inside the cavity, these astigmatic cavity configurations for which transverse modes become degenerate in finely spaced subgroups allow for the existence of more complex Lissajous patterns. Indeed, wave optics simulations in Fig. 3 are obtained at these special cavity lengths where mode crossings occur, which correspond to the finely spaced resonance peaks exemplified in Fig. 4(b).

In contrast to this behavior, for a spherical cavity a unique crossing occurs at L_r giving a single peak as visible in Fig. 4(a). Then, as L is changed from L_r , transverse modes with different $m+n$ order fan out with different slopes (remaining degenerate for constant $m+n$) given by $[(m+n)\partial\theta/\partial L]/2\pi$,

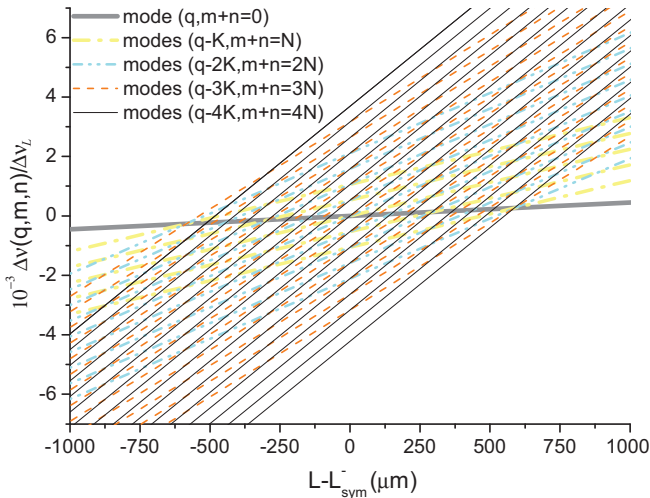


FIG. 5. (Color online) A portion of the “spectrum” of cavity resonances around the TEM_{00} mode, given by $\Delta\nu(q,m,n)/\Delta\nu_L$ as a function of the cavity detuning around L_{sym}^- for the first modes lying close to the TEM_{00} mode and having $m+n \leq 16$. $\Delta\nu(q,m,n)$ represents the frequency difference of the mode $\nu(q-i, iN)$ as a function of $L-L_{\text{sym}}^-$ for $0 \leq i \leq 4$, with respect to the fundamental mode $\nu(q,0,0)$ evaluated at $L=L_{\text{sym}}^-$. Simulations still involve $(N,K) = (4,1)$.

and cannot cross again in the neighborhood of L_r . While the previously degenerate groups of modes are breaking apart, the well-defined N -spots-on-an-ellipse Herriott pattern associated with the well-defined fractionally degenerate resonances disappear and, hence, a more and more irregular and dimmer “doughnut” shape is obtained.

Another interesting information provided by Fig. 5 is that the width of the degenerate region, where the effect of modes crossing can be observed, depends on the number of excited transverse modes: The higher the number of injected transverse modes (i.e., the more off axis the injection), the higher the number of successive Lissajous patterns obtained. Actually, only five crossings involve all the modes including the $(0,0)$ (unique thick gray line in the figure), but more crossings occur among higher-order modes for other cavity lengths.

Figure 5 helps to accurately determine the positions of the mode crossings, i.e., the cavity length detunings which allow to observe the successive sharp Lissajous patterns. Indeed, one can easily consider which transverse modes are involved in each of the crossings and write down the corresponding equations, which can be readily numerically solved with respect to the cavity length. Also, if one writes the equations for different pairs of transverse modes involved in a given multiple crossing, one finds that these simplify to the same equation. For example, to find all crossings of the $(0,0)$ mode with the $m+n=N$ modes, one has to impose $[\Delta\nu(0,0,0)/\Delta\nu_L] = [\Delta\nu(0, N/2-k, N/2+k)/\Delta\nu_L]$ with $k = -N/2, -N/2+1 \dots N/2$ (for even N). This simplifies to $(N/2-k)\theta_x(L, R_x) + (N/2-k)\theta_y(L, R_y) = 0$, for which solutions in the variable L are easily obtained numerically for each k . This same expression is found when considering the crossings of the $(0,0)$ mode with one-every-two modes of the family $m+n=2N$ (and in general, with one-every- i modes having $m+n=iN$). Again, the same expression results when

considering, for example, the crossings of the $n=m=N/2$ mode (the central of the yellow “dash dot” lines in Fig. 5) with the $m+n=2N$ modes, which actually confirms that the crossings in the figure “are” and do not just “appear” to be vertically aligned. From such calculations, in our case, we find that displacements $d_1 = -0.2932$ mm and $d_2 = 0.2927$ mm involve the crossing of the TEM_{00} mode with the modes $(3,1)$ and $(1,3)$, respectively, at closely symmetrical positions around L_{sym}^- , which above were considered to be equal and opposite cavity length changes by $\pm 2\Delta L$. We see therefore that in this respect Fig. 5 may be misleading, since the dependence of the Gouy phases on L is actually not perfectly linear so that the modes crossings and the Lissajous figures do not occur at perfectly equidistant ΔL values. This was previously assumed from empirical observation and from first modeling results, where the Lissajous patterns were found by manually varying the cavity length in the model and looking at the produced cavity output pattern. As we underlined earlier, the evolution of different modes with the same $m+n$ transverse order only appears to be given by parallel lines, but the slopes of these lines are actually slightly different, and a slight curvature is also present.

Together Figs. 4 and 5, and related discussions, lead to a generalization of the theory of reentrant spherical cavities to the astigmatic case. In the reentrant case, N -spot patterns are produced by the superposition of cavity transverse modes that are degenerate in N groups dividing the cavity FSR at equal frequency intervals [see Fig. 3(a)]. Indeed, running simulations as those giving the field patterns of Fig. 3 correctly reproduces, for each of the N degenerate groups of modes, the same pattern with N peaks on both mirrors [4]. Likewise in the astigmatic case, it is the formation of groups of degenerate cavity modes which allows the existence of the observed Lissajous field patterns. Again, scanning the frequency over the closely spaced degenerate groups of modes [see Fig. 4(b)], also produces always the same Lissajous figure at cavity output.

With respect to the values that the Gouy phases assume when the mode crossings occur, it turns out that these satisfy the relations $N\theta_x/2\pi - 1 = K_x$ and $N\theta_y/2\pi - 1 = K_y$, where K_x and K_y are positive (small) integers. In other words, the Gouy phases are close to $2\pi/N$ and their defects with respect to $2\pi/N$ are in a ratio of small integers. In addition, these integers correspond to the number of oscillations in the x and y transverse directions which characterize the generated closed Lissajous pattern.

Another point to note is that also configurations close to $d_1/2$ and $d_2/2$ (i.e., close to our initial $\pm\Delta L$ defined from observation) give multiple crossings in Fig. 5, but in this case each crossing does not involve all families of modes but just some of the families (every two families). As it can be seen in Fig. 2(d) from the patterns obtained by geometrical optics, these cases correspond to the appearance of less contrasted Lissajous profiles or, correspondingly, to the appearance of less contrasted peak structures in the cavity transmission spectrum as in Fig. 4(c).

This can be pushed further since we can see that there are also multiple mode crossings close to $d_1/3$ and $d_2/3$, but with each crossing involving modes from every three families and so on and so forth. At the end, however, intermediate cavity lengths in between the lower-order crossings give basically

no crossings or only involve modes of higher transverse order which at some point cannot even be excited given the finite transverse cavity size. The transmission function in frequency corresponds then to the case depicted in Fig. 4(c) for which the astigmatic cavity yields a disorganized transverse mode structure. Modeling with wave optics also consistently yields irregular, vague, and dimmer cavity output patterns at intermediate cavity lengths.

Additionally, it can be deduced from Fig. 5 that a central symmetrical pattern arises when the fundamental TEM_{00} mode is degenerate with symmetrical TEM_{mn} modes satisfying $m = n$. For example, the off-axis circulating intracavity field that causes the “X-O profiles” to be observed on the input and the output mirror at L_{sym}^- is found to result from the superposition of modes with $m = n = 2i$ where $i = 0, 1, 2, \dots, \infty$. Solving the corresponding equations yields the values L_{sym}^\pm also expressed by Eq. (5).

With respect to mode crossings occurring at symmetrical positions with respect to L_{sym}^- , for example, at the displacements d_1 and d_2 as considered before, we should remark that these are symmetric under the exchange of mode numbers m, n . We can finally understand the origin of the observed Lissajous patterns that appear basically rotated by 90° , even though the injection conditions are not generally subject to the same symmetry (except for some special choices of the incident off-axis beam). This also explains the differences that are visible when comparing such corresponding patterns generated at symmetric mode crossing positions around L_{sym}^- .

Finally, we underline that this analysis applies to any astigmatic cavity close to any N -fold reentrant configuration of the corresponding spherical cavity, with some slight differences. Thus, the central X-O pattern will not be of the same shape as here, and in the case of odd values of N the central crossing will not be a “complete” crossing involving all mode families, but a higher-order crossing of the type considered above for $d_1/2$ or $d_2/2$, which will appear not as sharp.

IV. CONCLUSION

In summary, we presented a complete description accounting for the observation of a succession of transverse Lissajous patterns at the output of an optical cavity with off-axis injection, over a small region of cavity lengths close to a N -fold reentrant configuration.

By first using geometrical optics, an intuitive understanding of the mechanism was provided: Because of a weak mirror

astigmatism and given a high-enough cavity finesse, Lissajous profiles are observed when the cavity length allows for oscillations of the impact coordinates on the two mirrors in the transverse directions (x, y) . For sufficiently high cavity finesse, the ray path may be able to complete a full Lissajous cycle, thus close onto itself, before complete extinction of the light intensity by cavity losses. In this case the beam impact points on the mirrors are able to draw a complete Lissajous pattern. This also explains why for a low-finesse cavity the small accidental mirror astigmatism is not sufficient to produce such kind of patterns, so that simple N -spots Herriott patterns are commonly observed in the reentrant case. Quantitative agreement with observation was found: Not only the modeled patterns match those observed as the cavity length is varied, but the positions where they occur are close to those experimentally determined, after the model is fed with a mirror astigmatism which is obtained from an independent measurement.

Excellent agreement with observation was then obtained by applying the wave optics approach developed in Ref. [4], which allowed further insight. With the help of this more complete and realistic representation based on transverse modes and the superposition principle [3], we have shown that Lissajous figures arise as soon as the transverse modes split by astigmatism become reorganized in frequency-degenerate subgroups clustered around the N resonant frequencies of the corresponding N -fold reentrant spherical cavity. Finally, a closer look at the specific modal dispersions associated with an astigmatic cavity allowed to explain the existence of a central profile around which is organized an intriguing spatial symmetry of the Lissajous profiles within the degenerate region.

This work represents a generalization of the theory of reentrant cavities to the astigmatic case and represents an application of the modeling framework based on transverse cavity modes proposed in [4]. It also illustrates the much deeper insight that wave optics modeling may provide with respect to a basic and more widely used geometrical optics approach.

ACKNOWLEDGMENTS

J.C. was supported by the French space agency “Centre National d’Etudes Spatiales.” The authors acknowledge useful discussions with Olivier Carraz during the preparation of this manuscript.

-
- [1] H. Kogelnik and T. Li, *Appl. Opt.* **5**, 1550 (1966).
 - [2] F. Bayer-Helmes, *Appl. Opt.* **23**, 1369 (1984).
 - [3] K. K. Lehmann and D. Romanini, *J. Chem. Phys.* **105**, 10263 (1996).
 - [4] D. Romanini, *Appl. Phys. B* (2013), doi: 10.1007/s00340-013-5632-x.
 - [5] D. R. Herriott, H. Kogelnik, and R. Kompfner, *Appl. Opt.* **3**, 523 (1964).
 - [6] D. R. Herriott and H. J. Schulte, *Appl. Opt.* **4**, 883 (1965).
 - [7] J. B. McManus, P. L. Kebabian, and M. S. Zahniser, *Appl. Opt.* **34**, 3336 (1995).
 - [8] Y. F. Chen, Y. P. Lan, and K. F. Huang, *Phys. Rev. A* **68**, 043803 (2003).
 - [9] Y. F. Chen, T. H. Lu, K. W. Su, and K. F. Huang, *Phys. Rev. Lett.* **96**, 213902 (2006).
 - [10] T. Klassen, J. de Jong, M. van Exter, and J. P. Woerdman, *Opt. Lett.* **30**, 1959 (2005).
 - [11] H. Huang and K. K. Lehmann, *Opt. Express* **15**, 8745 (2007).
 - [12] C. Bond, P. Fulda, L. Carbone, K. Kokeyama, and A. Freise, *Phys. Rev. D* **84**, 102002 (2011).
 - [13] J. Courtois, A. K. Mohamed, and D. Romanini, *Opt. Express* **18**, 4845 (2010).
 - [14] A. Yariv, *Quantum Electronics*, 3rd ed. (John Wiley & Sons, New York, 1989).